Feedback Linearization of an Underactuated Miniature Blimp with Zero Dynamics Mitigation using High Order Control Barrier Functions

Mihir Kasmalkar, *Graduate Student Member, IEEE*, Luke Baird, *Graduate Student Member, IEEE*, and Samuel Coogan, *Senior Member, IEEE*

Abstract— In this letter we derive a tracking controller based on feedback linearization for a miniature blimp controlled by co-located fans on an undermounted gondola. We prove that feedback linearization of the underactuated blimp induces nontrivial zero dynamics corresponding to lightly damped oscillations in pitch and roll. To mitigate these oscillations we use high-order control barrier functions (HOCBFs) to limit the maximum allowable pitch and roll at the expense of tracking error. Experimental results are presented for three illustrative trajectories which demonstrate that the proposed controller outperforms a well-tuned LQR controller and a baseline nonlinear MPC controller, while the attitude oscillations are theoretically and empirically shown to be bounded by the HOCBFs.

Index Terms— Feedback linearization, Autonomous systems, Robotics

I. INTRODUCTION

MINIATURE blimps are emerging as a promising aerial robotics platform. Due to their soft envelope, low-speed plastic propellers, and slow movement, they are often preferable to quadrotors for operation in confined spaces and in close proximity with people [1]. Furthermore, control strategies developed for miniature blimps are transferable to craft in other application domains, such as rigid dirigibles and marine vessels, which obey similar dynamics [2], [3].

Quadrotors are a common aerial vehicle platform with mature nonlinear control techniques, and it is natural to investigate whether these methods are transferable to blimps. The most successful nonlinear control strategies for quadrotors rely on feedback linearization and the very closely related property of differential flatness. The seminal paper [4] introduced a minimizing snap controller via full-state feedback linearization. The paper [5] develops a feedback linearization tracking controller that is robust to rotor faults by setting angular velocities as the flat outputs. Similarly, the paper [6] also develops a feedback linearization controller verified with
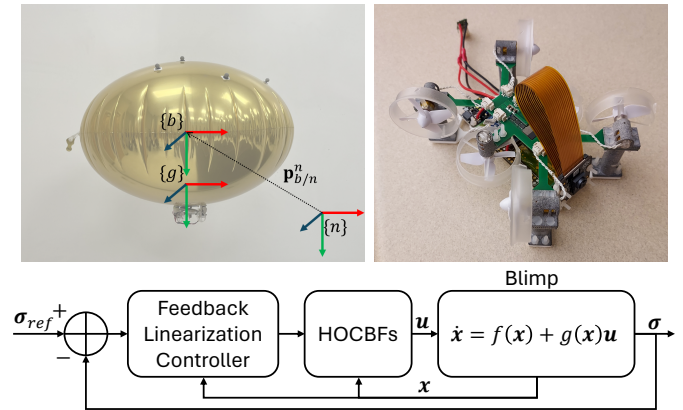
Fig. 1. Top: the Georgia Tech Miniature Autonomous Blimp (GT-MAB) with relevant coordinate frames (left) alongside the gondola electronics package displayed separately (right). The underactuated design of the radially symmetric blimp contributes to lightly damped zero dynamics under a feedback linearization-based controller, which we mitigate using HOCBFs. Bottom: the control architecture presented in this paper. Given a reference trajectory, we feedback linearize the system and then use HOCBFs to dampen oscillations.

experimental flight tests. The paper [7] selects outputs for state feedback linearization that leads to non-trivial zero dynamics, but dampens them with an outer loop high-level controller.

Although the dynamics of a radially symmetric blimp derived from Euler-Lagrange equations have the same state variables and the same type of control input (fan or rotor thrust) as a quadrotor, the dynamics are fundamentally distinct in that the control input directly couples the lateral and angular velocity dynamics [8].

In this letter, we show that a radially symmetric blimp with holonomic control is feedback linearizable but exhibits nontrivial zero dynamic oscillations in pitch and roll, a distinct phenomenon not present in quadrotor control. Furthermore, we develop a nonlinear tracking controller for the blimp based on feedback linearization. When feedback linearized, we show that the resulting zero dynamics are asymptotically stable but highly oscillatory, and we propose using control barrier functions (CBFs) to mitigate these oscillations, defined as limiting the maximum roll and pitch. We show that the relative degree from inputs to positional outputs is two, precluding the use of standard CBFs. Thus, we use high-order CBFs (HOCBFs) [9], [10] to limit the roll and pitch of the blimp. To

our knowledge, this letter is the first to empirically mitigate zero dynamics from feedback linearization using HOCBFs. Additionally, experimental results are presented in which the controller is shown to track a variety of trajectories while outperforming a well-tuned LQR controller and a nonlinear MPC controller.

A. Related Work

Several control strategies have been proposed for miniature blimps. Among them, linear optimal control strategies are a common solution, including [11] which proposes an MPC approach that models a blimp as double-integrator chains with time delay and [12] which uses Gaussian processes with a linear model to control an airship's yaw dynamics in a data-driven manner. However, these methods are fundamentally limited in that they rely on a linearized model, while the true dynamics are inherently nonlinear due to aerodynamic effects [2], [13].

Recent state-of-the-art controllers use nonlinear control techniques. Sliding-mode control [14] has commonly been used for trajectory tracking on blimps. Similarly, the paper [15] proposes an adaptive control method that decouples velocity and attitude control for trajectory tracking. The paper [16] develops a modern approach that combines a nonlinear MPC controller with a reinforcement learning agent. However, it is designed specifically for station-keeping while in this work we solve a trajectory tracking problem. Moreover, all of these methods require computational resources that are usually unavailable to a small blimp with a tight weight budget.

II. BLIMP DYNAMICS MODEL

We use the 6-DOF dynamical model of the blimp described in [13], which applies the general theory developed for marine craft in [2] to the specific case of the Georgia Tech Miniature Autonomous Blimp (GT-MAB) [13], a radially-symmetric blimp used in this letter's experiments. We briefly summarize this model next. The following conventions are used: A north-east-down [17] convention is used for all frames; the world frame n is fixed and has origin O at the center of a room on the floor; the body frame b is fixed to the blimp and is therefore translating and rotating with origin CB as the center of buoyancy of the blimp, which is the geometric center of the elliptical envelope. The center of gravity CG is located directly below the center of buoyancy aligned along the z-axis, and the corresponding frame g is fixed at the CG to the blimp like b. These frames are shown in Figure 1. The state vector $\mathbf{x} = (\boldsymbol{\nu}_{b/n}^b, \boldsymbol{\eta}_{b/n}^n) = (\mathbf{v}_{b/n}^b, \boldsymbol{\omega}_{b/n}^b, \mathbf{p}_{b/n}^n, \boldsymbol{\Theta}_{b/n}^n) \in \mathbb{R}^{12}$ is given by

$$\mathbf{v}_{b/n}^b = [v_x^b \ v_y^b \ v_z^b]^\top, \qquad \boldsymbol{\omega}_{b/n}^b = [\omega_x^b \ \omega_y^b \ \omega_z^b]^\top$$
$$\mathbf{p}_{b/n}^n = [x \ y \ z]^\top, \qquad \boldsymbol{\Theta}_{b/n}^n = [\phi \ \theta \ \psi]^\top,$$

which represents translational velocity in the body frame, angular velocity in the body frame, position in the world frame, and orientation of the blimp relative to the world frame, respectively.

Using rotation matrix $R_b^n(\mathbf{x})$ [2, Equation 2.31] and transformation matrix $T_b^n(\mathbf{x})$ [2, Equation 2.41], we relate the position and angular coordinates in the world frame to the translational and angular velocities in the body frame by

$$\dot{\boldsymbol{\eta}}_{b/n}^n = \begin{bmatrix} \dot{\mathbf{p}}_{b/n}^n \\ \dot{\boldsymbol{\Theta}}_{b/n}^n \end{bmatrix} = \begin{bmatrix} R_b^n(\mathbf{x}) & 0_{3\times3} \\ 0_{3\times3} & T_b^n(\mathbf{x}) \end{bmatrix} \begin{bmatrix} \mathbf{v}_{b/n}^b \\ \boldsymbol{\omega}_{b/n}^b \end{bmatrix}. \quad (1)$$

Note that $R_b^n(\mathbf{x})$ and $T_b^n(\mathbf{x})$ depend only on the Euler angles, and that $R_b^n(\mathbf{x})$ is always invertible while $T_b^n(\mathbf{x})$ is invertible except for a pitch of $\pm 90°$.

The input vector is $\mathbf{u} = (f_x^b, f_y^b, f_z^b, \tau_z^b) \in \mathbb{R}^4$, where f_x^b, f_y^b, and f_z^b are the thrust forces applied in the body frame x, y, and z directions at the gondola. τ_z^b is the torque applied about the body-frame z-axis. The blimp is underactuated and exhibits coupling between lateral thrust and angular acceleration. The complete vector of forces and torques $\boldsymbol{\tau}^b \in \mathbb{R}^6$ is thus given by

$$\boldsymbol{\tau}^b = \begin{bmatrix} 1 & 0 & 0 & 0 \\ 0 & 1 & 0 & 0 \\ 0 & 0 & 1 & 0 \\ 0 & -r_{z,t/g}^b & 0 & 0 \\ r_{z,t/g}^b & 0 & 0 & 0 \\ 0 & 0 & 0 & 1 \end{bmatrix} \begin{bmatrix} f_x^b \\ f_y^b \\ f_z^b \\ \tau_z^b \end{bmatrix} =: L\mathbf{u} \quad (2)$$

where $r_{z,t/g}^b$ is the z-component of the vector from the center of gravity to the point of application of the thrust forces (on the gondola), i.e. it is the moment arm about the center of gravity (CG) due to the thrust forces. Note that x-axis torque is caused by the moment generated by forces in the y direction, and vice-versa.

The full 6-DOF dynamics of the blimps are [2], [18]

$$\boldsymbol{\tau}^b = M^{CB}\dot{\boldsymbol{\nu}}_{b/n}^b + C^{CB}(\mathbf{x})\boldsymbol{\nu}_{b/n}^b + D^{CB}\boldsymbol{\nu}_{b/n}^b + G^{CB}(\mathbf{x}) \quad (3)$$

where M^{CB} is the the mass/inertia matrix, $C^{CB}(\mathbf{x})$ is the Coriolis-centripetal matrix, D^{CB} is the diagonal aerodynamic damping matrix, and the gravity vector is

$$G^{CB}(\mathbf{x}) = - \begin{bmatrix} 0_{3\times1} \\ \mathbf{r}_{g/b}^b \times \mathbf{f}_{g/b}^b \end{bmatrix}, \quad \mathbf{f}_g^b = (R_b^n(\mathbf{x}))^{-1} \begin{bmatrix} 0 \\ 0 \\ f_{z,g}^n \end{bmatrix}$$

where $f_{z,g}^n$ is the constant downward force of gravity and $\mathbf{r}_{g/b}^b = [0 \ 0 \ r_{z,g/b}^b]^\top$ is the vector position of the CG in the body frame, i.e. the vector from the CB to the CG. Acceleration due to gravity is zero because of the blimp's buoyancy, but gravity induces non-zero restoring torque about the CB.

We express these equations in a control-affine form as

$$\dot{\boldsymbol{\nu}}_{b/n}^b = K\mathbf{u} + N(\mathbf{x})\boldsymbol{\nu}_{b/n}^b + F(\mathbf{x}), \quad (4)$$
$$K = \left(M^{CB}\right)^{-1} L, \quad (5)$$
$$N(\mathbf{x}) = - \left(M^{CB}\right)^{-1} \left(C^{CB}(\mathbf{x}) + D^{CB}\right), \quad (6)$$
$$F(\mathbf{x}) = - \left(M^{CB}\right)^{-1} G^{CB}(\mathbf{x}). \quad (7)$$

Note that $N(\mathbf{x}) \in \mathbb{R}^{6\times6}$ and $F(\mathbf{x}) \in \mathbb{R}^{6\times1}$ are functions of state while $K \in \mathbb{R}^{6\times4}$ is independent of state.

We highlight the following constants that are referenced later in the paper for completeness: m_{RB} is the rigid body mass, I_x is the moment of inertia about the x-axis, and I_y is the moment of inertia about y-axis. These three terms appear in the mass/inertia matrix M^{CB}. Additionally, throughout this letter we use c$(\cdot)$, s$(\cdot)$ and t$(\cdot)$ as shorthand for $\cos(\cdot)$, $\sin(\cdot)$, and $\tan(\cdot)$, respectively.

III. Feedback Linearization Control Strategy

In this section we prove that the blimp dynamics are input-output feedback linearizable. Moreover, we demonstrate that under certain conditions, the zero dynamics of the system are locally asymptotically stable. The control architecture presented in this letter is outlined in Figure 1.

Theorem 1. *Consider the dynamical system (3). Take* $\boldsymbol{\sigma} = \begin{bmatrix} x & y & z & \psi \end{bmatrix}^\top$ *to be the output of the system and* $\mathbf{u} = \begin{bmatrix} f_x & f_y & f_z & \tau_z \end{bmatrix}^\top$ *to be the input. Suppose* $I_x, I_y \neq m_{RB}\, r^b_{z,g/b}\, r^b_{z,t/g}$. *Then, on the entire space space excluding states such that* $\mathrm{mod}\,(\theta, 2\pi) = \frac{\pi}{2}$ *or* $\mathrm{mod}\,(\phi, 2\pi) = \frac{\pi}{2}$, *this system is input-output feedback linearizable and has relative degree two for each output.*

Proof. First, we compute $\dot{x}, \dot{y}, \dot{z}$ by differentiating $\dot{\mathbf{p}}^n_{b/n}$ and $\dot{\psi}$ by differentiating $\dot{\boldsymbol{\Theta}}^n_{b/n}$, yielding

$$\ddot{\boldsymbol{\eta}}^n_{b/n} = \underbrace{\begin{bmatrix} R^n_b(\mathbf{x}) & 0_{3\times3} \\ 0_{3\times3} & T_\Theta(\mathbf{x}) \end{bmatrix}}_{J(\mathbf{x})} \dot{\boldsymbol{\nu}}^b_{b/n} + \underbrace{\begin{bmatrix} \dot{R^n_b(\mathbf{x})} & 0_{3\times3} \\ 0_{3\times3} & \dot{T}_\Theta \end{bmatrix}}_{\dot{J}(\mathbf{x})} \boldsymbol{\nu}^b_{b/n}.$$

Selecting the binary matrix $W \in \mathbb{R}^{4\times6}$ to pick out the second derivatives of the outputs, we find that

$$\ddot{\boldsymbol{\sigma}} = W\left(J(\mathbf{x})\dot{\boldsymbol{\nu}}^b_{b/n} + \dot{J}(\mathbf{x})\boldsymbol{\nu}^b_{b/n} \right).$$

Substituting (4),

$$\ddot{\boldsymbol{\sigma}} = W\left(J(\mathbf{x})\left(K\mathbf{u} + N(\mathbf{x})\boldsymbol{\nu}^b_{b/n} + F(\mathbf{x}) \right) + \dot{J}(\mathbf{x})\boldsymbol{\nu}^b_{b/n} \right).$$

Define the matrices $A(\mathbf{x}) \in \mathbb{R}^{4\times1}$ and $B(\mathbf{x}) \in \mathbb{R}^{4\times4}$ as

$$A(\mathbf{x}) := W\left(J(\mathbf{x})F(\mathbf{x}) + \left(J(\mathbf{x})N(\mathbf{x}) + \dot{J}(\mathbf{x}) \right)\boldsymbol{\nu}^b_{b/n} \right)$$
$$B(\mathbf{x}) := WJ(\mathbf{x})K.$$

Now, we can write $\ddot{\boldsymbol{\sigma}}$ using these matrices,

$$\ddot{\boldsymbol{\sigma}} = A(\mathbf{x}) + B(\mathbf{x})\mathbf{u}. \tag{8}$$

Note that the inverse $B(\mathbf{x})^{-1}$ is given by the expression

$$\begin{bmatrix} \frac{\star}{\beta_1} & \frac{\star}{\beta_1} & -\frac{\star}{\beta_1} & 0 \\ -\frac{\star}{\beta_2} & \frac{\star}{\beta_2} & \frac{\star}{\beta_2} & 0 \\ \star & \star & \star & 0 \\ \frac{\star}{\mathrm{c}(\phi)\,\beta_1} & \frac{\star}{\mathrm{c}(\phi)\,\beta_1} & -\frac{\star}{\mathrm{c}(\phi)\,\beta_1} & \frac{\star}{\mathrm{c}(\phi)} \end{bmatrix}$$

where $\beta_1 = I_y - m_{RB}\, r^b_{z,g/b}\, r^b_{z,t/g}$ and $\beta_2 = I_x - m_{RB}\, r^b_{z,g/b}\, r^b_{z,t/g}$. The numerators of the elements of $B(\mathbf{x})^{-1}$ have been omitted for brevity. It can be shown that $B(\mathbf{x})^{-1}$ exists by applying the assumptions of the theorem.

Define a fictitious input $\mathbf{q} := A(\mathbf{x}) + B(\mathbf{x})\mathbf{u}$ and solve for $\mathbf{u} = B(\mathbf{x})^{-1}(\mathbf{q} - A(\mathbf{x}))$. Then the second derivative of the outputs becomes $\ddot{\boldsymbol{\sigma}} = \mathbf{q}$. ∎

Next, we prove that with a proper design of the blimp parameters, the zero dynamics are locally asymptotically stable. To this end, we consider a linearization of the nonlinear zero dynamics about the origin and prove that the eigenvalues of the linearization lie in the open left-half complex plane for certain parameter values.

The following lemma characterizes these four-dimensional zero dynamics of the blimp which correspond to oscillations in roll and pitch.

Lemma 1. *Consider the system (3) with the input-output feedback linearization described in Theorem 1. The resulting zero dynamics are given by*

$$\dot{\phi} = \omega^b_x \qquad \dot{\theta} = \omega^b_y/\mathrm{c}\phi = -\omega^b_z/\mathrm{s}\phi \ (\textit{if } \phi \neq 0).$$

Proof. Since $\psi = \dot{\psi} = 0$,

$$\dot{\boldsymbol{\Theta}}^n_{b/n} = \begin{bmatrix} \dot{\phi} \\ \dot{\theta} \\ \dot{\psi} \end{bmatrix} = \begin{bmatrix} \dot{\phi} \\ \dot{\theta} \\ 0 \end{bmatrix} = T_\Theta(\mathbf{x})\begin{bmatrix} \omega^b_x \\ \omega^b_y \\ \omega^b_z \end{bmatrix}.$$

Multiplying the matrix $T_\Theta(\mathbf{x})$ out yields

$$\dot{\phi} = \omega^b_x + (\mathrm{s}\phi\mathrm{t}\theta)\,\omega^b_y + (\mathrm{c}\phi\mathrm{t}\theta)\,\omega^b_z \tag{9}$$
$$\dot{\theta} = (\mathrm{c}\phi)\,\omega^b_y - (\mathrm{s}\phi)\,\omega^b_z \tag{10}$$
$$0 = (\mathrm{s}\phi/\mathrm{c}\theta)\,\omega^b_y + (\mathrm{c}\phi/\mathrm{c}\theta)\,\omega^b_z. \tag{11}$$

We can simplify (9) by substituting in (11) yielding $\dot{\phi} = \omega^b_x$; to solve for $\dot{\theta}$, we substitute (11) into (10) to see that $\dot{\theta} = \omega^b_y/\mathrm{c}\phi$. If $\phi \neq 0$, substituting in (11) also yields $\dot{\theta} = -\omega^b_z/\mathrm{s}\phi$. ∎

Remark 1. *Note that ω^b_z is not necessarily zero, as intuition might suggest since $\dot{\psi} = 0$. Rather, we find that $\omega^b_z = -(\mathrm{t}\phi)\,\omega^b_y$. When ω^b_y is nonzero (equivalent to $\dot{\theta}$ being nonzero), there is a component of the angular velocity of the blimp in the direction of the body frame z-axis.*

To determine how the angular velocities evolve while the outputs and all of their derivatives are zero, we substitute $\mathbf{u} = -B(\mathbf{x})^{-1}A(\mathbf{x})$ into the velocity dynamics (4) giving

$$\dot{\boldsymbol{\nu}}^b_{b/n} = -KB(\mathbf{x})^{-1}A(\mathbf{x}) + N(\mathbf{x})\boldsymbol{\nu}^b_{b/n} + F(\mathbf{x}). \tag{12}$$

The angular velocity derivatives $\dot{\omega}^b_x$ and $\dot{\omega}^b_y$ are embedded in the vector $\boldsymbol{\nu}^b_{b/n}$. Thus, (12) describes the time-evolution of the angular velocities in the zero dynamics of the system and can be used to compute the relevant entries of the linearized system. We omit these expressions for brevity and present the key results—the eigenvalues of the linearized zero dynamics subsystem—in the following theorem.

Theorem 2. *Consider the system (3) with the input-output feedback linearization described in Theorem 1. If the inertias I_x and I_y satisfy $I_x, I_y > m_{RB}r^b_{z,g/b}r^b_{z,t/g}$, then the origin of the zero dynamics is locally asymptotically stable.*

Proof. We use the small angle approximation ($\mathrm{c}x \approx 1, \mathrm{s}x \approx x, \mathrm{t}x \approx x$) to linearize the zero dynamics about the origin. Specifically, we linearize the zero dynamics, where the original dynamics (3) are restricted to $\boldsymbol{\sigma} \equiv 0$. Let these dynamics be represented by $F_z(\mathbf{x}_z)$,

$$\dot{\mathbf{x}}_z = F_z(\mathbf{x}_z) \approx A_z\mathbf{x}_z$$
$$A_z \triangleq \frac{\mathrm{d}F_z}{\mathrm{d}\mathbf{x}_z}(0) \tag{13}$$
$$\mathbf{x}_z = \begin{bmatrix} \phi & \theta & \omega^b_x & \omega^b_y \end{bmatrix}^\top.$$

The matrix of partial derivatives A_z can be computed using the results from Lemma 1. The resulting matrix is

$$A_z = \begin{bmatrix} 0 & 0 & 1 & 0 \\ 0 & 0 & 0 & 1 \\ f_{31} & 0 & f_{33} & 0 \\ 0 & f_{42} & 0 & f_{44} \end{bmatrix}$$

where

$$f_{31} = \frac{-f_{z,g}^n r_{z,g/b}^b}{I_x - m_{RB} r_{z,g/b}^b r_{z,t/g}^b} \quad f_{33} = \frac{-D_{\omega,xy}^{CB}}{I_x - m_{RB} r_{z,g/b}^b r_{z,t/g}^b}$$

$$f_{42} = \frac{-f_{z,g}^n r_{z,g/b}^b}{I_y - m_{RB} r_{z,g/b}^b r_{z,t/g}^b} \quad f_{44} = \frac{-D_{\omega,xy}^{CB}}{I_y - m_{RB} r_{z,g/b}^b r_{z,t/g}^b}.$$

Here, we used the symmetry of the blimp about the z axis to note that $D_{\omega,xy}^{CB} = D_{\omega x}^{CB} = D_{\omega y}^{CB}$.

This system has eigenvalues

$$\begin{bmatrix} -\frac{D_{\omega,xy}^{CB} \pm \sqrt{D_{\omega,xy}^{CB\,2} + 4 f_{z,g}^n m_{RB} r_{z,t/g}^b r_{z,g/b}^{b\,2} - 4 I_x f_{z,g}^n r_{z,g/b}^b}}{2 \left(I_x - m_{RB} r_{z,g/b}^b r_{z,t/g}^b\right)} \\ -\frac{D_{\omega,xy}^{CB} \pm \sqrt{D_{\omega,xy}^{CB\,2} + 4 f_{z,g}^n m_{RB} r_{z,t/g}^b r_{z,g/b}^{b\,2} - 4 I_y f_{z,g}^n r_{z,g/b}^b}}{2 \left(I_y - m_{RB} r_{z,g/b}^b r_{z,t/g}^b\right)} \end{bmatrix}$$

Applying our assumption $I_x, I_y > m_{RB} r_{z,g/b}^b r_{z,t/g}^b$, the eigenvalues lie in the left-half complex plane. ∎

Remark 2. *These eigenvalues will lie in the open left-half plane if $I_x, I_y > m_{RB} r_{z,g/b}^b r_{z,t/g}^b$ and the dynamics will be oscillatory if $I_x, I_y > m_{RB} r_{z,g/b}^b r_{z,t/g}^b + D_{\omega,xy}^{CB\,2} / (4 f_{z,g}^n r_{z,g/b}^b)$. This justifies the intuition that if the inertia of the blimp is sufficiently large, the steady-state torques due to the applied forces $u = -B^{-1}A$ will not induce sufficient acceleration to overcome the restoring torque and induce instability. However, if the inertia of the blimp is too large, then any non-zero initial pitch or roll condition will result in overshoot and lightly damped oscillations. The eigenvalues were found to satisfy the above conditions for realistic blimp parameters, including those of the GT-MAB.*

IV. CONTROLLER DESIGN WITH HIGH-ORDER CONTROL BARRIER FUNCTIONS

To achieve a desired steady-state velocity during operation, a minimum pitch or roll angle is required to balance the restoring torque [8]. Using the proposed feedback linearization based controller, the effect of this pitch/roll angle is to introduce increasingly oscillatory zero dynamics as the speed of the trajectory increases especially if overshoot occurs, an effect which is exaggerated under parametric uncertainty or actuator saturation. This is a direct consequence of the underactuated design of the gondola yielding the structure of the matrix L in (2). While one solution is to decrease the speed of the trajectory, a preferable alternative is to design a controller which will minimally deviate from the action of the nominal feedback linearization controller while ensuring that the pitch and roll angles do not exceed unacceptable limits. Thus, we use control barrier functions (CBFs) to limit the allowable oscillations in roll and pitch.

To implement CBFs, we combine the dynamics of (1) and (4) in a control-affine form, $\dot{\mathbf{x}} = f(\mathbf{x}) + g(\mathbf{x})\mathbf{u}$. We select barrier functions

$$h_\phi(\mathbf{x}) = \frac{1}{2}\left(-\phi^2 + \phi_{\text{limit}}^2\right) \quad h_\theta(\mathbf{x}) = \frac{1}{2}\left(-\theta^2 + \theta_{\text{limit}}^2\right)$$

These functions are nonnegative when the respective variable lies within the specified bounds, *e.g.* $h_\phi(\mathbf{x}) \geq 0$ iff $\phi \in [-\phi_{\text{limit}}, \phi_{\text{limit}}]$. However, for each of these functions, the Lie derivative along the vector field $g(\mathbf{x})$ is identically zero. Thus, the following barrier functions [9], [10] are used:

$$\Psi_i(\mathbf{x}) = L_f h_i(\mathbf{x}) + \gamma_i h_i(\mathbf{x}) \quad i \in \{\phi, \theta\}.$$

The Lie derivatives of each of these functions along g are zero at some points. At these points, the remaining terms in the CBF program constraint are

$$L_f \Psi_\phi + \gamma_\phi \Psi_\phi = \frac{\gamma^2 \phi_{\text{limit}}^2}{2} - \left(w_x^b + \mathsf{t}\theta\, w_z^b\right)^2$$

$$L_f \Psi_\theta + \gamma_\theta \Psi_\theta = \frac{\gamma^2 \theta_{\text{limit}}^2}{2} - \left(\mathsf{c}\phi\, w_y^b - \mathsf{s}\phi\, w_z^b\right)^2$$

These terms are nonnegative (and the CBF constraint is satisfied) if the angular velocities are sufficiently small. In practice, this condition was always met, and infeasibility of the optimization program was not encountered during experimental tests.

We note that the issue where $L_g \Psi_{\theta,\phi} = 0$ at some points could be avoided by applying methods in [19], [20] or choosing quartic instead of quadratic barrier functions $h_{\theta,\phi}$. Specifically, we could instead choose

$$h_\phi'(\mathbf{x}) = \frac{1}{4}\left(-\phi^4 + \phi_{\text{limit}}^4\right) \quad h_\theta'(\mathbf{x}) = \frac{1}{4}\left(-\theta^4 + \theta_{\text{limit}}^4\right)$$

However, in both simulation and hardware experiments we never encountered this issue and thus used the proposed barriers $h_{\phi,\theta}$ for numerical simplicity.

To incorporate the CBFs into the controller for the blimp, we define the following optimization program to compute the actual input $\mathbf{u}^*$ which will be applied,

$$\mathbf{u}^* = \arg\min_{\boldsymbol{\mu}} ||\boldsymbol{\mu} - \mathbf{u}(\mathbf{x})||_2^2$$

$$\text{s.t. } L_f \Psi_\theta(\mathbf{x}) + L_g \Psi_\theta(\mathbf{x})\boldsymbol{\mu} \geq -\gamma_\theta \Psi_\theta(\mathbf{x})$$

$$L_f \Psi_\phi(\mathbf{x}) + L_g \Psi_\phi(\mathbf{x})\boldsymbol{\mu} \geq -\gamma_\phi \Psi_\phi(\mathbf{x})$$

where γ_θ and γ_ϕ are positive constants.

The overall control architecture is as follows: state feedback is used to compute the nominal input required to stabilize the integrator chains comprising the feedback linearized system, and a quadratic program is then solved to find the input which minimally deviates from this nominal controller in order to ensure positive invariance of the safe set defined by the CBFs. Recall that $\boldsymbol{\sigma}$ and $\dot{\boldsymbol{\sigma}}$ contain the states of the integrator chains resulting from the feedback linearization and that $\ddot{\boldsymbol{\sigma}}$ is equal to the control input $\mathbf{q}$. Namely, $\boldsymbol{\sigma} = [x\ y\ z\ \psi]^\top$, $\dot{\boldsymbol{\sigma}} = [\dot{x}\ \dot{y}\ \dot{z}\ \dot{\psi}]^\top$, and $\ddot{\boldsymbol{\sigma}} = \mathbf{q}$. Let $\mathbf{y}_d$ be the reference trajectory: $\mathbf{y}_d = [x^{\text{ref}}\ y^{\text{ref}}\ z^{\text{ref}}\ \psi^{\text{ref}}]^\top$. Define $\mathbf{e}$ to be the system error: $\mathbf{e} = \boldsymbol{\sigma} - \mathbf{y}_d$, which implies that $\dot{\mathbf{e}} = \dot{\boldsymbol{\sigma}} - \dot{\mathbf{y}}_d$ and $\ddot{\mathbf{e}} = \mathbf{q} - \ddot{\mathbf{y}}_d$. We can stabilize the integrator chains by defining $\mathbf{q}$ via state feedback with gains k_1 and k_2 (in the general MIMO case, a matrix K) selected appropriately to ensure that the dynamics matrix of the closed-loop system is Hurwitz: $\mathbf{q} = -k_1 \mathbf{e} - k_2 \dot{\mathbf{e}} + \ddot{\mathbf{y}}_d$. The nominal control input is thus $\mathbf{u}(\mathbf{x}) = B(\mathbf{x})^{-1}\left(\mathbf{q} - A(\mathbf{x})\right)$ with $\mathbf{q}$ defined as above.

Remark 3. *Provided that the bandwidth of the control loop is sufficiently high, actuator saturation does not occur, and no*

points where $L_g\Psi_{\theta,\phi} = 0$ are encountered (except when $\theta, \phi = 0$), the controller given by $\mathbf{u}^*$ will keep the roll and pitch angles within specified limits. This follows from [9, Theorem 5] and was empirically observed in simulation.

Remark 4. *Our procedure is applicable to any control-affine nonlinear system with well-defined relative degree and lightly-damped asymptotically stable zero dynamics. However, a trade-off emerges between trajectory tracking performance and zero dynamics damping. Zero dynamics, by definition, will always exist if the state of the feedback linearized system (defined in trajectory following applications as the tracking error) remains identically at zero. By modifying the nominal action of the feedback linearization controller to reduce the zero dynamics oscillations, the state must therefore deviate from the origin, and tracking performance is degraded.*

V. Experimental Results

Hardware experiments were performed to characterize the proposed controller under slow trajectories which would not violate the CBF boundary as well as fast trajectories which required the CBFs. The control algorithm was run on a benchtop computer which communicated over a 2.4 GHz connection with the blimp. The blimp was retrofitted with reflective markers to enable the real-time collection of state data using an OptiTrack motion capture system[1].

The GT-MAB uses a helium-filled envelope for buoyancy and is equipped with a 3D-printed gondola with a Raspberry Pi Zero 2 W, IMU, six lightweight thrusters, motor board custom PCB, and a battery [8]. Four lateral and two vertical counter-rotating thrusters permit holonomic control. Control actions are computed on a lab computer and are relayed over a network connection to the on-board custom PCB. Position, velocity, attitude, and angular velocity state data is collected using an OptiTrack motion capture system and on-board IMU.

Three trajectories were selected for experimental testing: a line, a circular helix, and a sawtooth-like series of triangular z-axis translations while the blimp moves laterally in a square. The proposed feedback linearization-based controller was implemented to follow these trajectories with optional CBF limits of 5° on ϕ and θ. Note that these trajectories were sufficiently slow that, while the CBFs were enabled, they were rarely active, demonstrating the capability of the underlying feedback linearization controller. The CBF quadratic program was solved with Gurobi for our feedback linearization controller. We additionally implemented two controllers for comparison: an LQR controller with gain matrices determined by Bryson's Rule [21], and a Nonlinear MPC [22] algorithm with a 10 step (0.5s) horizon and hand-tuned cost matrix minimizing tracking error. All control loops were run at 20Hz. The average computation time required by the LQR controller was 0.3 ms, feedback linearization 1.0 ms, feedback linearization+CBF 9.87 ms, and finally NMPC 63.9 ms. For every trajectory, three trials were done using each control strategy and the average values of selected performance metrics are tabulated in Table
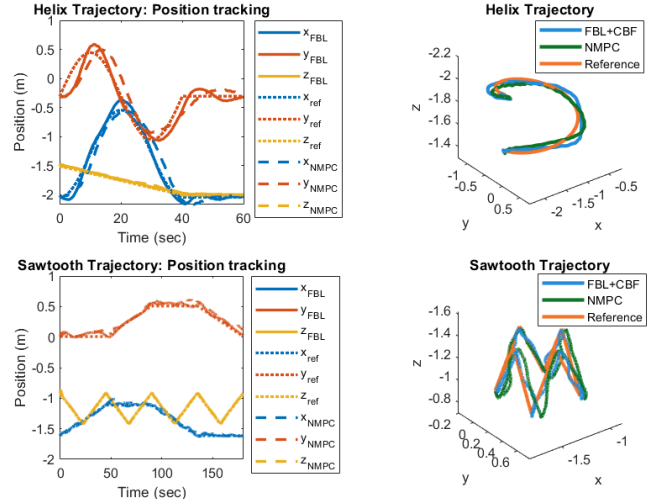
Fig. 2. Tracking a helical and sawtooth trajectory using the proposed feedback linearization-based controller with HOCBFs for zero dynamics damping on physical hardware. The CBF parameter is $\gamma_\phi = \gamma_\theta = 10$ for the helix trajectory and $\gamma_\phi = \gamma_\theta = 1$ for the sawtooth trajectory. The CBF limit is set to 5°, and the attitude oscillations did not exceed this limit. The nonlinear MPC trajectory is plotted for a visual comparison.

Experiment	Pos. Error	ψ Error	Pk. θ	Pk. ϕ
FBL+CBF, Line	0.0428 m	0.7234°	1.7381°	2.3452°
LQR, Line	0.0766 m	1.4702°	1.4796°	4.0809°
NMPC, Line	0.0737 m	1.3810°	2.2390°	3.5070°
FBL+CBF, Helix	0.1352 m	1.5061°	2.3561°	2.2190°
LQR, Helix	0.1221 m	4.1411°	2.2157°	5.4025°
NMPC, Helix	0.2375 m	3.7629°	2.7816°	3.6289°
FBL+CBF, Sawtooth	0.0345 m	0.5864°	1.9895°	1.7607°
LQR, Sawtooth	0.0946 m	2.0743°	1.6922°	5.3107°
NMPC, Sawtooth	0.0704 m	1.3670°	1.3982°	1.7154°

TABLE I

Comparison of Proposed FBL vs. LQR and NMPC RMS Errors

I. Plots of experimental results are found in Figure 2. We note that the computation times are consistent with the complexity of each controller. LQR requires a matrix multiplication, FBL requires a matrix inversion and multiplication, FBL+CBF uses a QP to apply the CBF, and NMPC solves a nonlinear program.

From Table I we see that the feedback linearization controller has less position tracking and yaw error than both the LQR controller and the NMPC controller, while the roll and pitch oscillations do not exceed the 5° limit.

While both the feedback linearization and NMPC controllers suffer from model mismatch, we see that the feedback linearization controller is empirically able to compensate more effectively. We observe that this is due to feedback linearization requiring far less compute than NMPC, and therefore is able to meet the 20Hz control loop deadline consistently unlike NMPC. In simulation we can artificially remove computational limits and use a smaller discretization step and longer MPC horizon, empirically achieving a position error of 0.04 m along the helix trajectory for NMPC. However, this is not realizable on hardware again due to computational constraints.

To illustrate the effectiveness of the CBFs, we then increased the speed of the line and sawtooth trajectories to induce greater oscillations. The effects of the CBFs are depicted in Figure 3. For the line trajectory, the speed of the control
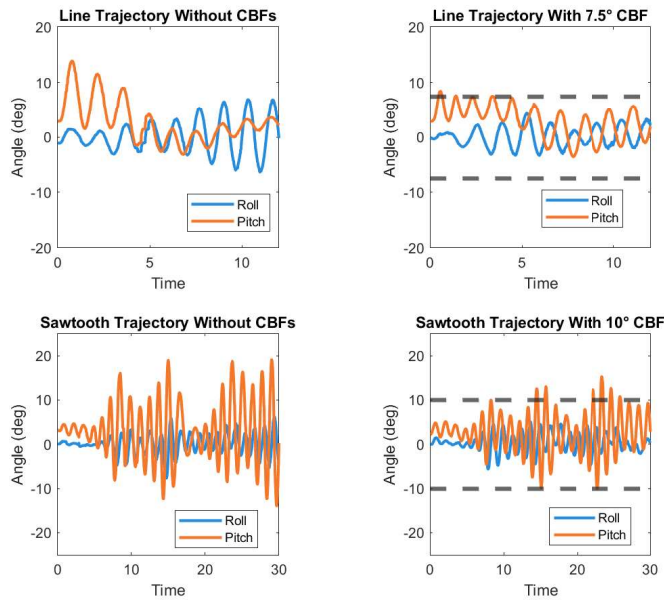
Fig. 3. When the speed of the trajectory is increased, HOCBFs mitigate the maximum roll and pitch observed. For both trajectories, the CBF parameter is $\gamma_\phi = \gamma_\theta = 10$. While actuator saturation and control loop bandwidth limitations prevent the roll and pitch from remaining strictly within the boundaries, the CBFs noticeably decrease the zero dynamics oscillations.

loop was increased to 100 Hz, while it remained at 20 Hz for the triangular trajectory. The zero dynamics are observed to be bounded by the CBF limits, with brief excursions which likely arise due to actuator saturation and control bandwidth limitations; these excursions do not manifest when simulated without actuator or bandwidth restrictions. This is acceptable since the condition that the roll and pitch do not exceed the boundaries is not a safety requirement, but rather a performance objective.

Remark 5. *If the conditions of Remark 3 are not satisfied, the controller may not be able to prevent violation of the CBF limit. Additionally, if the required control input is too large, the system may temporarily violate CBF boundaries due to actuator saturation. Both of these phenomena were observed during hardware experiments while simulations without actuation and bandwidth limitations demonstrated that the zero dynamics remained properly bounded.*

VI. Conclusion

We performed feedback linearization of a miniature blimp actuated by an undermounted gondola and described its lightly damped oscillatory zero dynamics. We then formulated HOCBFs that mitigate its oscillatory dynamics. Experimental results demonstrate that the proposed controller outperforms a baseline LQR and NMPC implementation while achieving acceptable damping of the zero dynamics. The proposed algorithm may be implemented within a nested architecture in which higher-level controllers, such as MPC or a runtime assurance layer [23], prescribe a trajectory and rely on the feedback linearization controller to accomplish low-level trajectory following. We seek to implement this architecture on hardware in future work, applying a high-level controller while formally guaranteeing safety.

References

[1] N. Yao, Q. Tao, W. Liu, Z. Liu, Y. Tian, P. Wang, T. Li, and F. Zhang, "Autonomous flying blimp interaction with human in an indoor space," *Frontiers of Information Technology & Electronic Engineering*, vol. 20, no. 1, pp. 45–59, 2019.

[2] T. I. Fossen, *Handbook of marine craft hydrodynamics and motion control*. John Wiley & Sons, 2011.

[3] G. Antonelli, S. Chiaverini, N. Sarkar, and M. West, "Adaptive control of an autonomous underwater vehicle: experimental results on odin," in *Proceedings 1999 IEEE International Symposium on Computational Intelligence in Robotics and Automation*, 1999, pp. 64–69.

[4] D. Mellinger and V. Kumar, "Minimum snap trajectory generation and control for quadrotors," in *2011 IEEE international conference on robotics and automation*. IEEE, 2011, pp. 2520–2525.

[5] A. Freddi, A. Lanzon, and S. Longhi, "A feedback linearization approach to fault tolerance in quadrotor vehicles," *IFAC proceedings volumes*, vol. 44, no. 1, pp. 5413–5418, 2011.

[6] D. Lee, H. Lee, J. Lee, and D. H. Shim, "Design, implementation, and flight tests of a feedback linearization controller for multirotor uavs," *International Journal of Aeronautical and Space Sciences*, vol. 18, no. 4, pp. 740–756, 2017.

[7] L. Martins, C. Cardeira, and P. Oliveira, "Feedback linearization with zero dynamics stabilization for quadrotor control," *Journal of Intelligent & Robotic Systems*, vol. 101, no. 1, pp. 1–17, 2021.

[8] Q. Tao, J. Wang, Z. Xu, T. X. Lin, Y. Yuan, and F. Zhang, "Swing-reducing flight control system for an underactuated indoor miniature autonomous blimp," *IEEE/ASME Transactions on Mechatronics*, vol. 26, no. 4, pp. 1895–1904, 2021.

[9] W. Xiao and C. Belta, "Control barrier functions for systems with high relative degree," in *2019 IEEE 58th conference on decision and control (CDC)*. IEEE, 2019, pp. 474–479.

[10] ——, "High-order control barrier functions," *IEEE Transactions on Automatic Control*, vol. 67, no. 7, pp. 3655–3662, 2021.

[11] H. Fukushima, K. Kon, Y. Hada, F. Matsuno, K. Kawabata, and H. Asama, "State-predictive control of an autonomous blimp in the presence of time delay and disturbance," in *2007 IEEE International Conference on Control Applications*. IEEE, 2007, pp. 188–193.

[12] J. Ko, D. J. Klein, D. Fox, and D. Haehnel, "Gaussian processes and reinforcement learning for identification and control of an autonomous blimp," in *Proceedings 2007 ieee international conference on robotics and automation*. IEEE, 2007, pp. 742–747.

[13] Q. Tao, M. Hou, and F. Zhang, "Modeling and identification of coupled translational and rotational motion of underactuated indoor miniature autonomous blimps," in *16th International Conference on Control, Automation, Robotics and Vision*. IEEE, 2020, pp. 339–344.

[14] M. Wasim, A. Ali, M. A. Choudhry, I. Shaikh, and F. Saleem, "Robust design of sliding mode control for airship trajectory tracking with uncertainty and disturbance estimation," *Journal of Systems Engineering and Electronics*, vol. 35, no. 1, pp. 242–258, 2024.

[15] Z. Meng, J. Ma, and T. Zhang, "Adaptive fast trajectory tracking control for the airship based on prescribed performance," *Proceedings of the Institution of Mechanical Engineers, Part G: Journal of Aerospace Engineering*, pp. 893–908, 2024.

[16] M. A. Escarcega, T. Doyle, and M. Hassanalian, "Adaptive weight tuning of a model predictive controller for a stratospheric airship using reinforcement learning," in *AIAA AVIATION FORUM AND ASCEND 2024*, 2024, p. 3897.

[17] P. D. Groves, *Principles of GNSS, inertial, and multisensor integrated navigation systems (2nd edition)*. Artech house, 2013.

[18] Q. Tao, J. Tan, J. Cha, Y. Yuan, and F. Zhang, "Modeling and control of swing oscillation of underactuated indoor miniature autonomous blimps," *Unmanned Systems*, vol. 9, no. 01, pp. 73–86, 2021.

[19] J. Breeden and D. Panagou, "Robust control barrier functions under high relative degree and input constraints for satellite trajectories," *Automatica*, vol. 155, p. 111109, 2023.

[20] A. J. Taylor, P. Ong, T. G. Molnar, and A. D. Ames, "Safe backstepping with control barrier functions," in *2022 IEEE 61st Conference on Decision and Control (CDC)*. IEEE, 2022, pp. 5775–5782.

[21] J. Hespanha, *Linear systems theory*. Princeton university press, 2018.

[22] J. Rawlings, D. Mayne, and M. Diehl, *Model Predictive Control: Theory, Computation, and Design*. Nob Hill Publishing, LLC, 2022.

[23] L. Baird and S. Coogan, "Runtime assurance from signal temporal logic safety specifications," in *American Control Conference (ACC)*, 2023, pp. 3535–3540.